Clays and Clay Minerals, Vol. 43, No. 4, 391–396, 1995.

MODEL CALCULATION OF SEPIOLITE SURFACE AREAS

TOSHIYUKI HIBINO,[1] ATSUMU TSUNASHIMA,[1] ATSUSHI YAMAZAKI,[2] AND RYOHEI OTSUKA[2]

[1] Materials Processing Department, National Institute for Resources and Environment
16-3 Onogawa, Tsukuba, 305 Japan

[2] Department of Mineral Resources Engineering, School of Science and Engineering,
Waseda University, 3-4-1 Ohkubo, Shinjyuku, 169 Japan

Abstract—In general, the N_2-BET surface areas of sepiolite samples range from 95 to 400 m^2/g depending on deposits.

The surface areas of five sepiolites, all varying in crystallite size, were measured on heating, and were compared with a model calculation. A sharp decrease in the surface area, due to crystal folding, was observed between 200° and 400°C. Both before and after the folding, each sepiolite sample had peculiar values. Our model sufficiently explains this difference in surface areas among the samples. In the model, which is based on the Brauner-Preisinger structural model, surface area is a function of the crystallite size and the ratios of the coverage for nitrogen adsorption on both the internal and external surfaces. These ratios of the coverage can be inversely estimated from the model. The ratios of the coverage on the internal surface are less than 0.19, and that on the external surface between 0.7 and 1.0.

Key Words—Heat treatment, Model calculation, Sepiolite, Surface area.

INTRODUCTION

The crystal structure of sepiolite, a hydrous magnesium silicate mineral with a fibrous morphology, has been established by Nagy and Bradley (1955), and Brauner and Preisinger (1956). The structure includes continuous silica tetrahedral sheet inverts apical direction at regular intervals, and talc-like ribbons. Each talc-like ribbon alternates with channels along the fiber axis. The channels refer to structural micropores, which give sepiolite its large surface area. The BET surface areas with nitrogen were reported from 95 to 400 m^2/g (Nishimura *et al* 1972, Sarikaya 1981).

The surface area of sepiolite will change upon heating (Nishimura *et al* 1972, Dandy and Nadie-Tabbiruka 1975, Grillet *et al* 1988). Sepiolite transforms to sepiolite anhydride on heating to 300°C. All adsorbed and zeolitic water and half of the coordination water are lost up to 300°C (Serna *et al* 1975). Simultaneously, crystal folding occurs: opposite ribbons approach each other by alternating rotations. When sepiolite is heated in air, the surface area scarcely changes up to 200°C. However, a sharp decrease occurs between 200° and 400°C, above which the surface area becomes almost constant. This sudden drop of the surface area is caused by the crystal folding. In the case of heating in vacuo, the decrease of the surface area starts and ends at a lower temperature (150°–250°C) than in air.

Although previous works reported almost the same transition temperature, there are considerable differences among various samples with regards to their maximum and minimum surface areas. The cause for these differences was assumed to be a result of differences in the particle size distribution, crystal imperfections and impurities (Nishimura *et al* 1972, Dandy and Nadiye-Tabbiruka 1982, Inagaki *et al* 1990). This assumption however was not derived from empirical data. In the present study, we calculated the surface areas of sepiolite from the structural model and crystallite size, and then compared the calculated surface areas with the BET surface areas.

EXPERIMENTAL

Materials

The sepiolite samples used were from five different deposits. These samples are identified by the name of the deposit, as shown in Table 1. The impurities detected by X-ray powder diffraction (XRD) were removed by elutriation. After which, the samples were dried, and ground to 100–150 mesh.

Heat treatment and the measurement of surface area

Sample masses of about 0.2 g were dried at 100°C for 8 h, and then heated in air for 2 h at 100°, 150°, 200°, 250°, 300°, 350°, 400°, 450°, 500° and 650°C. To prevent rehydration, the samples were put into cells while the samples were hot. The cells were then stuffed with glasswool. Samples were weighed together with the cells. The surface areas of the samples were calculated from the adsorption isotherm of nitrogen by using the BET method. Prior to the measurement, the samples were outgassed at 100°C for two hours.

The measurement of crystallite size and other analyses

The crystallite size of sepiolite in the direction of [110] was determined from the integral width of the (110) diffraction peak by using Scherrer's equation. The profile of the diffraction peak was corrected for instrumental broadening, using zeolite as a standard.

Table 1. Structural formula of sepiolite from various deposits.

Sample	Deposit	Dehydrated structural formula (half unit cell)
Imisehir	Imisehir, Turkey	$(Si_{11.82}Al_{0.04})Mg_{8.25}O_{32}(Ca_{0.01}Na_{0.02}K_{0.03})$
Kanan	Kanan, China	$(Si_{11.89}Al_{0.06})Mg_{8.09}O_{32}(Ca_{0.01}Na_{0.05}K_{0.03})$
Korea	Korea	$(Si_{11.76}Al_{0.17}Fe^{3+}_{0.05})Mg_{8.01}O_{32}(Ca_{0.09}Na_{0.05}K_{0.04})$
Kuzuu	Kuzuu, Japan	$(Si_{11.82}Al_{0.12})Mg_{8.12}O_{32}(Na_{0.05}K_{0.04})$
Vallecas	Vallecas, Spain	$(Si_{11.58}Al_{0.42})[Al_{0.09}Fe^{3+}_{0.06}Ti_{0.01}Mg_{7.71}]_{7.87}O_{32}(Ca_{0.17}Na_{0.06}K_{0.15})$

The morphology of sepiolite was observed with a transmission electron microscope (TEM). Finally, the chemical composition was determined by inductively coupled plasma emission spectrochemical analysis (ICP).

RESULTS

Table 1 gives structural formulae of sepiolites calculated from the results of the chemical analysis. The structural formulae of sepiolite samples were close to the ideal formula based on the Brauner-Preisinger model ($Si_{12}Mg_8O_{32}$: dehydrated phase), however Vallecas-sepiolite contained a little more Al than other samples did.

Figure 1 shows the N_2-BET surface area for samples as a function of heating temperature. Starting values of the surface areas ranged from 170 to 320 m^2/g. The sharp decrease of surface areas occurred between 200° and 400°C, at which crystal folding occurred. The surface areas decreased to 30–40% of the starting values. Beyond 400°C, the surface areas remained practically constant, and each sample had a particular value of surface area. Although the surface areas above 400°C were almost constant, they decreased slightly between 450° and 650°C. This may be attributed to loss of structure water and sintering of the crystallite.

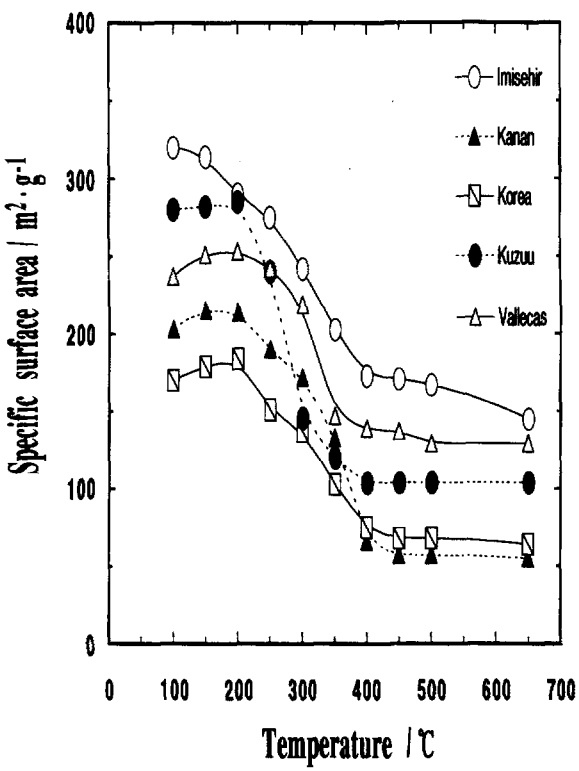

Figure 1. The surface areas of sepiolite heated at various temperatures.

DISCUSSION

It is obvious from the above results shown that sepiolites differ in surface area among samples, both before and after the crystal folding. In this section, we calculate the surface area based on a structural model. The model calculation is then compared with the measured surface areas.

Model calculation

Figure 2 shows an electron micrograph of a cross section whose shape is rhombic. The cross section models in Figure 3 are based on Figure 2 as well as the Brauner and Preisinger structural model; Figure 3a is a model before the crystal folding, and 3b after the crystal folding. Using the model in Figure 3a, we can calculate the surface area of crystalline fibers in a 1 g-sepiolite. The surface areas prior to the folding is given as,

$$S_{unfolded} = [2 \times a/2 \times b/2 \times N_r + 4 \cdot D'L + 2 \times (a/2 + b/2) \cdot N_c \cdot L] \times N_{cry} \quad (1)$$

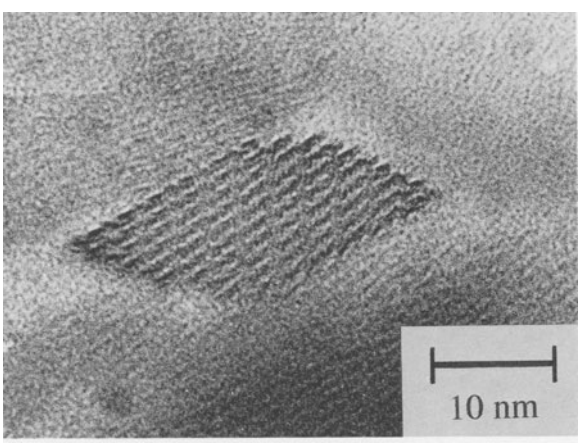

Figure 2. The electron micrograph of sepiolite. Section normal to the fiber axis (Kuzuu-sepiolite).

https://doi.org/10.1346/CCMN.1995.0430401 Published online by Cambridge University Press

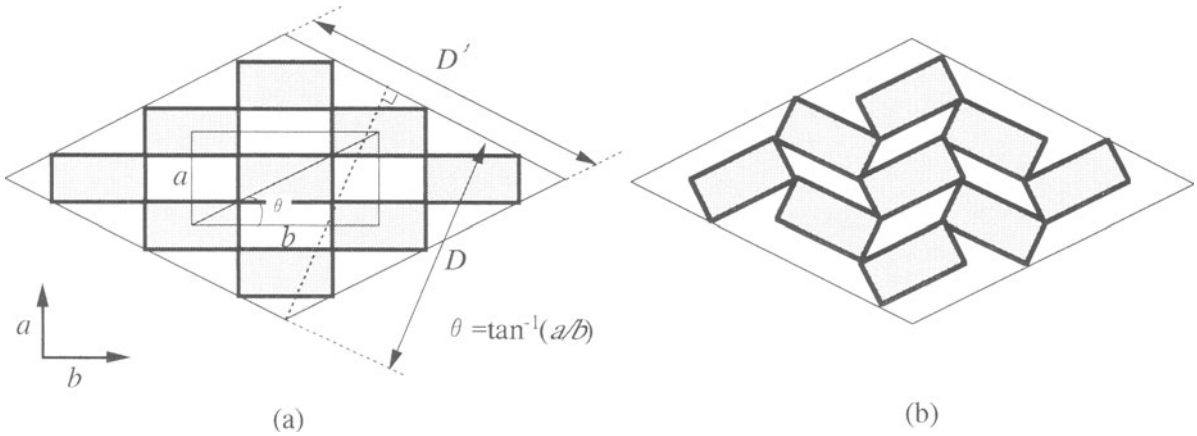

Figure 3. A model of the cross section (a) prior to the folding and (b) posterior to the folding. The talc-like ribbons are dotted.

where:

a, b and c = lattice constants on the basis of an orthorhombic cell [a = 1.34, b = 2.68, c = 0.53 nm (Brauner and Preisinger 1956)]
L = the length of the crystalline fiber
N_r and N_c = the number of talc-like ribbons and channels in a crystallite
N_{cry} = the number of crystallites in a 1 g-sepiolite sample
D′ = the length of a side of rhombic cross section for a crystalline fiber, as shown in Figure 3.

Regarding the calculation, the internal surface area of the channels distinguishes it from the external surface area. In Eq. (1), the first and second terms represent the external surface area, and the third the internal surface area. The first term is the cross section of the talc-like ribbons. This is the area subtracted the cross section of the channels from the total cross section. The second is the side area of the crystalline fiber. We can calculate the cross section as a rhombus approximately, not step-like shape, as are shown in Figure 3a. Geometrically, slightly more nitrogen molecules can adsorb on the step-like shape than on the rhombus shown in Figure 3a and 3b. Nevertheless, the molecules sited on corners, which are unstable positions, are also counted for the step-like shape. Hence, the actual number of adsorbed molecules on sepiolite sample must be less than that of the step-like shape model, and close to that of the rhombus model.

After the folding occurs, the channels are not accessible to the nitrogen molecules, since the width of the channels in the direction of *a* axis becomes less than the diameter of the nitrogen molecules. Consequently, the internal surface area is not measured by the BET method after the folding, and the term of the internal surface area is then deleted from Eq. (1). The rhombus of the cross section is unchanged by the folding, as shown in Figure 3. Then, the surface area after the folding is

$$S_{folded} = (2 \times D' \cdot D + 4D' \cdot L) \times N_{cry} \quad (2)$$

where D is the crystallite size in the direction normal to (110) plane, as shown in Figure 3.

The first term in Eq. (2) is the area of this rhombus. After the folding, it is not necessary to subtract the cross section of the channels from the area of this rhombus. The second term in Eq. (2) is the side area of the crystalline fiber as well as in Eq. (1).

In Eqs. (1) and (2), the crystallite size D and lattice constants a, b and c are determined by XRD. The length of a crystalline fiber L is observed with TEM. If the values of D′, N_r, N_c and N_{cry} are obtained experimentally, the surface area is calculated concretely using the Eqs. (1) and (2). These values can be derived from a, b, c, D and L as follows.

The length of a side of rhombic cross section D′ is determined geometrically by

$$D' = D/\sin 2\theta \quad (3)$$

where θ is $\tan^{-1}(a/b) = 26.57$. Therefore,

$$D' = D/0.8 \quad (4)$$

The number of talc-like ribbons in a crystallite N_r is obtained from the cross section of the crystalline fiber $D \cdot D'$ divided by the size of unit cell $a \cdot b$, considering the number of talc-like ribbons in a unit cell.

$$N_r = DD'/ab \times 2 = 2D^2/(ab \sin 2\theta) \quad (5)$$

The number of channels in a crystallite N_c is related to N_r as

$$N_c/N_r = (n_r - 1)^2/n_r^2 = (n_r^2 - 2n_r + 1)/n_r^2 \quad (6)$$

where n_r is the number of the talc-like ribbons on a

https://doi.org/10.1346/CCMN.1995.0430401 Published online by Cambridge University Press

side of the rhombus that is shown in Figure 3. The value of n_r equals $\sqrt{N_r}$, Eq. (6) is then rewritten

$$N_c = N_r - 2\sqrt{N_r} + 1 \quad (7)$$

The number of crystallites in a 1 g-sepiolite sample N_{cry} is the reciprocal of the mass of a crystallite, which is represented by the mass of a talc-like ribbon multiplied by N_r. Then

$$N_{cry} = c/(m_r \cdot N_r \cdot L) \quad (8)$$

where m_r is the mass of the talc-like ribbon that has the length of c in the direction of the fiber axis. These values of m_r are calculated on the basis of the Brauner and Preisinger model, as the value of m_r prior to the folding is 1.91×10^{-21} g, and posterior to the folding 1.79×10^{-21} g. Substituting equation (4), (5), (7) and (8) in Eqs. (1) and (2), we obtain

$$S_{unfold} = [4.98/L + 19.93/D + (11.15 - 26.74/D + 16.02/D^2)] \times 10^2 \quad (9)$$

$$S_{folded} = [10.63/L + 21.27/D] \times 10^2 \quad (10)$$

where the values of S_{unfold} and S_{folded} are expressed in m^2/g and the values of L and D in nm.

Empirically, the value of D is no more than 40 nm, and the value of L is more than 1 μm. Hence, the value of 1/L is so small compared with the values of 1/D and $1/D^2$ that Eqs. (9) and (10) can be approximated to

$$S_{unfold} = [19.93/D + (11.15 - 26.74/D + 16.02/D^2)] \times 10^2 \quad (11)$$

$$S_{folded} = 21.27/D \times 10^2 \quad (12)$$

Considering for nitrogen adsorption

The surface areas calculated from Eq. (11) are much larger than the areas measured using the BET method, though the values from Eq. (12) are slightly larger than the measured ones. For example, S_{unfold} is 1092 m^2/g compared with the BET surface area of 170 m^2/g, and S_{folded} 78 m^2/g with 64 m^2/g for Korea-sepiolite. All surface area is accessible to the nitrogen molecules in Eqs. (11) and (12). Actually, there are the surfaces that are not accessible to the nitrogen molecules, such as the internal surface of closed channels and the external surface cohering between the crystallites. Furthermore, the channels are so small that the nitrogen molecules are not capable of penetrating into the channels easily. Hence, the Eqs. (11) and (12) can be rewritten in the form including the correction

$$S^*_{unfold} = [19.93/D \times f_{ex} + (11.15 - 26.74/D + 16.02/D^2) \times f_{in}] \times 10^2 \quad (13)$$

$$S^*_{folded} = 21.27/D \times f_{ex} \times 10^2 \quad (14)$$

where f_{ex} is the ratio of coverage for the nitrogen adsorption on the external surface, and f_{in} for that on the internal surface.

The value of f_{ex} means the degree of dispersion for the crystallites. The nitrogen molecules are adsorbed only on the outside of the cohering crystallites. The external surface area then decreases, compared to the external surface area when there is no coherence. Therefore, f_{ex} can be written as

$$f_{ex} = s^*_{out}/s_{out} \quad (15)$$

where s^*_{out} is the external surface area of an actual sample that has coherence, and s_{out} the external surface area of the crystallites. The value of s^*_{out} also means the external surface area measured with the BET method.

Regarding f_{in}, it is deduced that the value of f_{in} is less than 0.19 from the sizes of the channel and the nitrogen molecule. The dimension of the cross section for the channel is approximately estimated at a/2 × b/2 from the Brauner and Preisinger model. However, the width along the *a* axis is accurately more narrow than a/2 by the radii of the oxygen on both sides, and the width along the *b* axis by the radii of the bound water molecules on both sides. Because the channel is completed by the oxygen sheets in the direction of the *a* axis, and by the bound water molecules in the direction of the *b* axis. The cross section is then (a/2 − 0.14 × 2) × (b/2 − 0.14 × 2) nm, viz. 0.39 × 1.06 nm. Here, we assume that the van der Waals radius of oxygen is 0.14 nm, and the radius of the bounded water molecule is the same as that of oxygen; the O-H bond would prefer to be oriented parallel to the *c* axis. On the other hand, taking into account the radius of hydrogen and covalent bond distance of O-H, the cross section of the channel is 0.39 × 0.91 nm.

For the nitrogen molecule, two sizes are also derived. One is calculated as a sphere from the density of liquid nitrogen and the molecular weight. Its diameter is 0.43 nm and is used in the BET method. The other is calculated as a dumbbell-like shape from the van der Waals radius and covalent bond distance, and is 0.31 × 0.42 nm. For either size, the width along the *a* axis is almost equal to the size of the nitrogen molecule. It is then doubtful that the nitrogen molecules are capable of penetrating into the channel. Nevertheless, it is obvious by the study of Inagaki *et al* (1990) that migration and filling are possible. They measured the BET surface area of sepiolite with various adsorbates. We conclude that the nitrogen molecule has a dumbbell-like shape, and that they can penetrate the channel with their shorter axis along the *a* axis. Then, the nitrogen molecules are filled in one row in the direction of the *a* axis, and in two rows in the direction of the *b* axis. On the *bc* plane of the channel, we assumed that the projection of the nitrogen molecule was a circle with a diameter of 0.42 nm, because the nitrogen molecules

https://doi.org/10.1346/CCMN.1995.0430401 Published online by Cambridge University Press

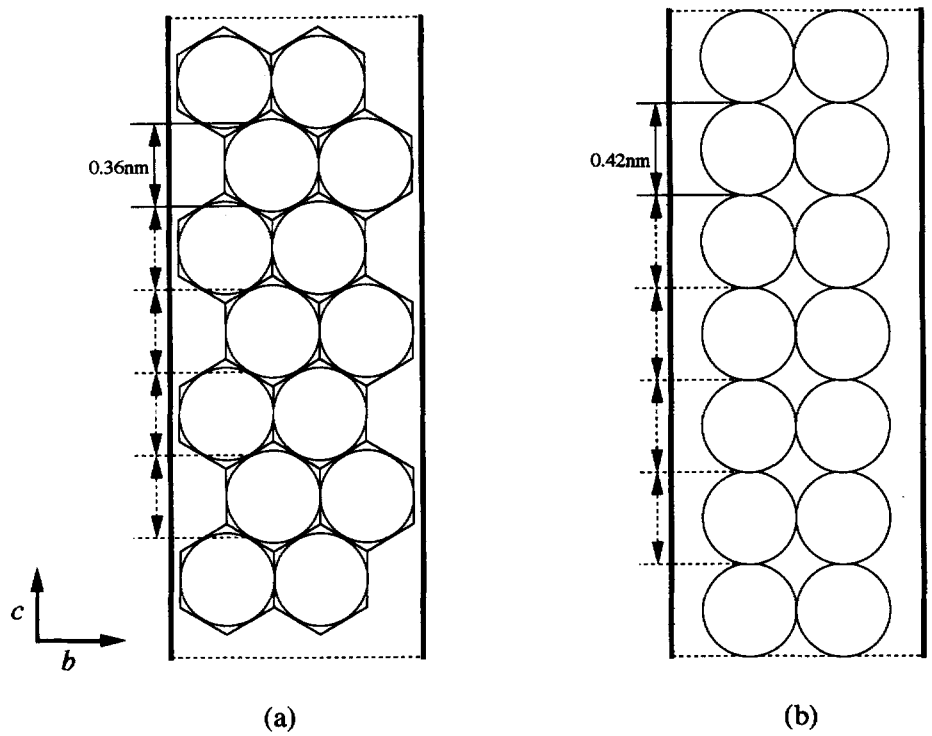

Figure 4. A schematic illustration of the nitrogen adsorption into a channel of sepiolite on the plane normal to *a* axis. The circles are nitrogen atoms. In BET method, the area covered by a nitrogen molecule is regarded as the hexagon drawing in this figure. The channel is outlined by the thicker lines.

could rotate. Along the *c* axis, two types of stacking are possible. One type is the closest packing; the molecules of the second layer fit into holes between the molecules of the first layer, and the molecules of the third layer fall into holes of the second layer and over the molecules of the first layer. This sequence is repeated indefinitely, as is shown in Figure 4a. The nitrogen molecules are packed closest in this fashion, and the layers stack at the intervals of 0.36 nm. The other type of stacking has two lines as shown in Figure 4b. The interval of the layer is 0.42 nm in this stacking. In the former manner of stacking, 1.05 nm, which is the width 2.5 times as long as the diameter of the nitrogen molecule, is indispensable along the *b* axis. This size is exactly the former width of the channel, and is larger than the latter. Therefore, it is difficult and unlikely for the nitrogen molecules to stack in this fashion. We then adopt the latter manner of stacking. Thus, the number of adsorption sites in the channels in a 1 g-sepiolite sample N^*_{in} is given as

$$N^*_{in} = 2 \times (L/0.42) \times N_c \times N_{cry} \qquad (16)$$

On the other hand, the internal surface area in Eq. (1) is calculated geometrically, and the van der Waals radii and the relation in size between the channels and nitrogen molecules are not taken into account. Since the area that a nitrogen molecule cover on an adsorbent is 0.162 nm^2 in the BET method, N_{in} that is the number of the adsorption sites on the internal surface area in Eq. (1) is given as

$$N_{in} = 2 \times (a/2 + b/2) \times Nc \times L \times N_{cry}/0.162 \qquad (17)$$

Then the ratio of N^*_{in}/N_{in} is 0.19, and this is the value of f_{in}. Actually, the value of f_{in} will be less than or equal to 0.19, because there are some closed channels by crystal defects or imperfections.

This discussion concerned with f_{in} is applicable to the thoroughly low relative pressure where the adsorption isotherm fits to the BET equation. The BET sur-

Table 2. The crystallite size, the specific surface area and the ratio of the coverage on the surface.

Sample	*D*/nm	BET surface area/$m^2 \cdot g^{-1}$		Ratio of coverage on the surface	
		Prior folding	Posterior folding	f_{in}	f_{ex}
Imisehir	9.1	320	171	0.19	0.73
Kanan	37.5	203	57	0.14	1.00
Korea	27.2	170	68	0.10	0.87
Kuzuu	17.6	280	104	0.19	0.86
Vallecas	13.3	237	137	0.12	0.86

The BET surface area of the sample heated at 100°C is adopted for the surface area prior to the folding, and that heated at 450°C posterior to the folding.

https://doi.org/10.1346/CCMN.1995.0430401 Published online by Cambridge University Press

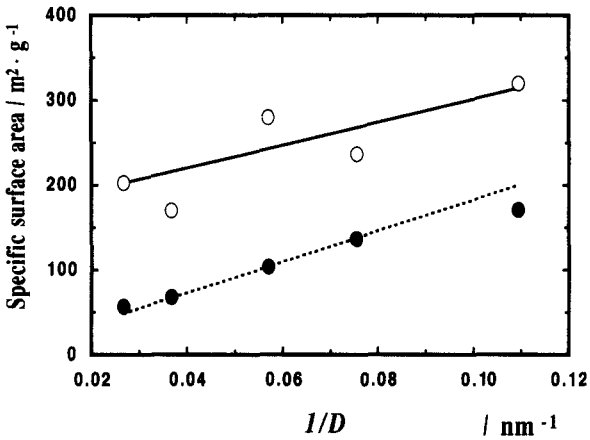

Figure 5. Comparison of the calculated and measured surface areas as a function of inverse crystallite site 1/D. The solid line is the calculated value prior to the folding, and dotted line posterior to the folding. The BET surface areas measured prior to the folding (100°C) is represented by open circles, and those posterior to the folding (450°C) closed circles.

face area of sepiolite decreases at the range of higher relative pressure when the ratio of filling in the channels is high, because the multilayer adsorption as is assumed in the BET theory does not occur in the channels.

Comparison of calculated and measured surface areas

We can measure the crystallite size, and the surface areas both before and after the crystal folding. We therefore derived the value of f_{ex} and f_{in} from Eqs. (13) and (14) for each sample. Table 2 lists these results. The value of f_{in} of each sample is less than or equal to 0.19, as is expected in the discussion above. Furthermore, the value of f_{ex} of Kanan-sepiolite is 1.00. This suggests that there is little coherence of the crystallites.

Since the values of f_{ex} and f_{in} were scattered within a more narrow range than the values of D, the average values of f_{ex} and f_{in} are adopted as a standard value, and substituted in Eqs. (13) and (14). Figure 5 shows the relation between the calculated surface areas and the measured ones in a function of inverse crystallite size 1/D. The calculated values sufficiently fit the measured ones. Consequently, the difference of the surface area among sepiolite samples is mainly explained by the difference of the crystallite size.

CONCLUSION

On the basis of the Brauner and Preisinger structural model, we calculated the surface area of sepiolite. The surface areas are given as:

before the crystal folding;

$$S^*_{unfold} = [19.93/D \times f_{ex} + (11.15 - 26.74/D + 16.02/D^2) \times f_{in}] \times 10^2$$

and after the crystal folding;

$$S^*_{folded} = 21.27/D \times f_{ex} \times 10^2$$

where, the values of S^*_{unfold} and S^*_{folded} are expressed in m^2/g and the values D in nm. The value of D is the Scherrer crystallite size in the direction normal to (110) plane. The value of f_{ex} is the ratio of the coverage for the nitrogen adsorption on the external surface and f_{in} that on the internal surface.

These equations fit the BET surface areas of five sepiolite samples that differ in surface area and crystallite size, when the average values of f_{ex} and f_{in} are substituted.

ACKNOWLEDGMENTS

The authors greatly thank Professor T. Watanabe for analyzing the chemical compositions of sepiolites with ICP. Dr. A. Ito is also thanked for discussions of this study.

REFERENCES

Brauner, K., and A. Preisinger. 1956. Struktur und Entstehung des Sepioliths. *Tschermaks Miner. Petr. Mitt.* **6**: 120–140.

Dandy, A. J., and M. S. Nadiye-Tabbiruka. 1975. The effect of heating in vacuo on the microporosity of sepiolite. *Clays & Clay Miner.* **23**: 428–430.

Dandy, A. J., and M. S. Nadiye-Tabbiruka. 1982. Surface properties of sepiolite from Amboseli, Tanzania, and its catalytic activity for ethanol decomposition. *Clays & Clay Miner.* **30**: 347–352.

Grillet, Y., J. M. Cases, M. Francois, J. Rouquerol, and J. E. Poirier. 1988. Modification of the porous structure and surface area of sepiolite under vacuum thermal treatment. *Clays & Clay Miner.* **36**: 233–242.

Inagaki, S., Y. Fukushima, H. Doi, and O. Kamigaito. 1990. Pore size distribution and adsorption selectivity of sepiolite. *Clay Miner.* **25**: 99–105.

Nagy, B., and W. F. Bradley. 1955. The structural scheme of sepiolite. *Amer. Mineral.* **40**: 885–892.

Nishimura, Y., Y. Hori, and H. Takahashi. 1972. Structural change and adsorption character of sepiolite by heat treatment. *J. Clay Sci. Soc. Japan* **12**: 102–108.

Sarikaya, Y. 1981. Effect of outgassing temperature on surface area of sepiolite. *Commun. Fac. Sci. Univ. Ankara, Ser. B* **27**: 45–49.

Serna, C., J. L. Ahlrichs, and J. M. Serratosa. 1975. Folding in sepiolite crystals. *Clays & Clay Miner.* **23**: 452–457.

(Received 1 July 1994; accepted 21 October 1994; Ms. 2531)